bioRxiv preprint doi: https://doi.org/10.1101/591461; this version posted March 27, 2019. The copyright holder for this preprint (which was not certified by peer review) is the author/funder, who has granted bioRxiv a license to display the preprint in perpetuity. It is made available under aCC-BY-NC 4.0 International license.

Aboave-Weaire's law in epithelia results from an angle constraint in contiguous polygonal lattices

Roman Vetter[1,2,†], Marco Kokic[1,2,†], Harold Gómez[1,2], Leonie Hodel[1], Bruno Gjeta[1], Antonella Iannini[3], Gema Villa-Fombuena[3], Fernando Casares[3], Dagmar Iber[1,2,*]

Affiliations:

[1] Department of Biosystems, Science and Engineering (D-BSSE), ETH Zurich, Mattenstrasse 26, 4058 Basel, Switzerland

[2] Swiss Institute of Bioinformatics (SIB), Mattenstrasse 26, 4058 Basel, Switzerland

[3] CABD, CSIC-Universidad Pablo de Olavide, Seville, Spain.

[†] The authors contributed equally.

* Corresponding author: Dagmar Iber dagmar.iber@bsse.ethz.ch

Keywords: Epithelial Organisation, Aboave-Weaire's Law, Surface Energy, Computational Model

bioRxiv preprint doi: https://doi.org/10.1101/591461; this version posted March 27, 2019. The copyright holder for this preprint (which was not certified by peer review) is the author/funder, who has granted bioRxiv a license to display the preprint in perpetuity. It is made available under aCC-BY-NC 4.0 International license.

ABSTRACT:

It has long been noted that the cell arrangements in epithelia, regardless of their origin, exhibit some striking regularities: first, the average number of cell neighbours at the apical side is (close to) six. Second, the average apical cell area is linearly related to the number of neighbours, such that cells with larger apical area have on average more neighbours, a relation termed Lewis' law. Third, Aboav-Weaire's (AW) law relates the number of neighbours that a cell has to that of its direct neighbours. While the first rule can be explained with topological constraints in contiguous polygonal lattices, and the second rule (Lewis' law) with the minimisation of the lateral contact surface energy, the driving forces behind the AW law have remained elusive. We now show that also the AW law emerges to minimise the lateral contact surface energy in polygonal lattices by driving cells to the most regular polygonal shape, but while Lewis' law regulates the side lengths, the AW law controls the angles. We conclude that global apical epithelial organization is the result of energy minimisation under topological constraints.

bioRxiv preprint doi: https://doi.org/10.1101/591461; this version posted March 27, 2019. The copyright holder for this preprint (which was not certified by peer review) is the author/funder, who has granted bioRxiv a license to display the preprint in perpetuity. It is made available under aCC-BY-NC 4.0 International license.

INTRODUCTION

Epithelia are polarized tissues. This means that cell properties change along the apical-basal axis (Fig. 1a). In particular, cells adhere tightly on the apical side via an adhesion belt composed of Cadherins, while they bind to the extracellular matrix on the basal side. When viewed from the apical side, the tissue appears as a contiguous polygonal lattice (Fig. 1b). The organisation of the polygonal lattice may appear random at first sight, but it has previously been noted to follow certain phenomenological laws. First, even though the fraction of cells with a certain number of neighbours differs hugely between epithelial tissues (Fig. 1c), the average number of neighbours, $\bar{n}$, is always close to six (Fig. 1d) [1-7] because of topological constraints in 2D contiguous polygonal lattices [4, 8]. In fact, in the limit of an infinite number of polygons, the average number of neighbours is exactly

$$\bar{n} = 6, \tag{1}$$

if three cells meet at each vertex; this can be derived from Euler's formula, v-e+f =2, which formulates a relationship between the number of vertices, v, edges, e, and faces, f. Second, the average apical area is linearly related to the number of cell neighbours, n, a relation termed Lewis' law (Fig. 1e), i.e.

$$\frac{\overline{A_n}}{\bar{A}} = \frac{n-2}{4} \tag{2}$$

Here, $\overline{A_n}$ refers to the average apical area of cells with n neighbours, and $\bar{A}$ refers to the average apical area of all cells in the tissue. We have recently shown that Lewis' law can be explained with a minimisation of the lateral cell-cell contact surface energy (Kokic et al, submitted). The lateral contact surface energy is minimal if the cell-cell contact area, and thus the combined cell perimeter is minimised. For a given apical area, the cell perimeter is minimal if the polygons are the most regular. To form a contiguous polygonal lattice from regular polygons, these need to all have the same side/edge length. However, for the same polygon area, side lengths differ between polygon types (Fig. 1f). In epithelial tissues, apical areas vary as a result of several processes, most prominently growth

bioRxiv preprint doi: https://doi.org/10.1101/591461; this version posted March 27, 2019. The copyright holder for this preprint (which was not certified by peer review) is the author/funder, who has granted bioRxiv a license to display the preprint in perpetuity. It is made available under aCC-BY-NC 4.0 International license.

and cell division. By following the relationship between polygon area and polygon type as stipulated by Lewis' law (Eq. 2), the difference in side lengths is minimised between cells. However, equal side lengths are only achieved if the areas followed a quadratic rather than a linear relationship,

$$\frac{\overline{A_n}}{\bar{A}} \approx \left(\frac{n}{6}\right)^2. \tag{3}$$

This quadratic relationship only emerges in case of a larger variability in apical areas than previously observed in epithelia. We confirmed this prediction by increasing the area variability in the *Drosophila* larval wing disc, which led to the predicted quadratic relationship (Kokic et al, submitted).

Finally, Aboav-Weaire's law (AW law) formulates a relationship between the number of neighbours, n, that a cell has and the average number of neighbours, m_n, of its direct neighbours (Fig. 1g). Aboav [9] empirically observed for grains in a polycrystal that

$$m_n \cdot n = 5n + 8. \tag{4}$$

Eq. 4 has previously been found to be a close approximation to the neighbour relationships in epithelial tissue in both plants [10-12] and animals [7] (Fig. 1h). However, Eq. 4 cannot explain regular hexagonal packings, where $m_6 = 6 \neq 5 + \frac{8}{6}$. Weaire suggested a refinement of the form

$$m_n \cdot n = 5n + 6 + Var(n), \tag{5}$$

where $Var(n) = \sum_{n=3}^{\infty}(n - \bar{n})^2 f_n$ is the variance of the polygon distribution, and f_n is the fraction of cells with n neighbours [13]. Eq. 5 applies to hexagonal lattices as $Var(n) = 0$, and reduces to Eq. 4 for $Var(n) = 2$. Efforts to explain the mathematical basis of Eqs. 4 and 5 have led to a wide range of

bioRxiv preprint doi: https://doi.org/10.1101/591461; this version posted March 27, 2019. The copyright holder for this preprint (which was not certified by peer review) is the author/funder, who has granted bioRxiv a license to display the preprint in perpetuity. It is made available under aCC-BY-NC 4.0 International license.

alternative formulations [14], but no physical or mathematical argument has so far been established to explain the experimental observations.

In the following, we will show that the emergence of the AW law in epithelia can be explained with the minimisation of the lateral contact surface energy. We previously showed that Lewis' law ensures that the side lengths of the different polygon types are the most similar, so that the different polygon types can fit within a polygonal lattice as the most regular polygons. To form a regular polygon also the internal angles of the polygon must match the polygon type, and to form a contiguous lattice, the internal angles around the shared vertex of adjacent cells must add to 360°. We show that this second constraint results in the AW law.

RESULTS

The emergence of the AW law can be explained with the minimisation of lateral surface energy

In the first step, we sought to test whether the AW law could be explained with the minimisation of the lateral contact surface energy. We have previously introduced the simulation framework `LBIBCell` [15] to simulate epithelial tissues (Kokic et al, submitted). `LBIBCell` represents tissues in a 2D plane, and can thus be used to simulate the apical tissue dynamics (Fig. 2a). The simulation framework offers high spatial resolution, i.e., it represents the boundaries of all cells separately such that cells can unbind and the spatial resolution is sufficiently high that cell edges can be curved. Cortical tension as well as cell-cell adhesion are implemented via springs between vertices. The fluid inside and outside the cells is represented explicitly and the fluid dynamics are approximated by the Lattice Boltzmann method. The interaction between the elastic cell boundaries and the fluid is realised via an immersed boundary condition.

bioRxiv preprint doi: https://doi.org/10.1101/591461; this version posted March 27, 2019. The copyright holder for this preprint (which was not certified by peer review) is the author/funder, who has granted bioRxiv a license to display the preprint in perpetuity. It is made available under aCC-BY-NC 4.0 International license.

The biological parameters in the simulation are the growth rate, the cell division threshold (i.e. the apical cell area, at which the cell divides), as well as the spring constants representing cortical tension and cell-cell adhesion. We have previously adjusted these to recapitulate the quantitative data from the *Drosophila* larval wing disc, a model epithelial tissue, and we have re-used the same setup as described before (Kokic et al, submitted; Supplementary Material, Table S1). When we simulate the *Drosophila* larval wing disc dynamics while dividing cells either perpendicular to their longest axis (Hertwig's rule [16]) (Fig. 2b, orange line) or randomly (Fig. 2b, cyan line), the resulting lattice results in polygonal relationships that are close to the AW law (Fig. 2b, black line). The deviation of the simulations from the AW law is similar to that observed for epithelial tissues (Fig. 2c). Thus, if we determine the parameters a and b for which

$$m_n \cdot n = a \cdot n + b \tag{5}$$

best fits the simulations and the data, the inferred values differ in a similar way from those of the AW law (a=5, b=8) [9]. We note that the b parameter deviates more than the a parameter. Weaire linked the b parameter to the variance in the observed polygon distribution, i.e. $b = 6 + Var(n)$ (Eq. 5) [13]. However, $6 + Var(n)$ does not correlate with the parameter b that we infer from the data (Fig. 2d), thus ruling out such a relationship. Given the definition of variance, the hexagon fraction declines with the variance of the polygon distribution (Fig. 2e), and $Var(n) = 2$ and thus $b = 8$ as in Aboav's formulation is observed only for tissues with low hexagon fraction (~30%), which are rare (Fig. 1c).

We conclude that the `LBIBCell` simulations generate a distribution of cell-cell contacts that lead to similar parameters for the AW law as observed in epithelia, but that differ from those specified by Aboav and Weaire. This suggests that the AW law could be explained with a minimisation of the lateral contact surface energy. But why would energy minimisation result in neighbour arrangements that follow the AW law?

bioRxiv preprint doi: https://doi.org/10.1101/591461; this version posted March 27, 2019. The copyright holder for this preprint (which was not certified by peer review) is the author/funder, who has granted bioRxiv a license to display the preprint in perpetuity. It is made available under aCC-BY-NC 4.0 International license.

Perfect polygonal lattices do not follow Aboav's law, but match Weaire's law

To understand the underlying constraint that leads to the particular form of the AW law, we consider perfect polygonal lattices made of regular polygons. The simplest case is a perfect hexagonal lattice (Fig. 3a, red). Here, all polygons must have the same area. To generate other regular lattices, cells with the appropriate areas must be placed in the correct relative position within the polygonal lattice. The relative areas of the different polygon types must follow the quadratic law (Eq. 3) so that all polygons in the lattice have the same side length. In addition, the internal angles of the cells that meet at a vertex must add up to 360° (Fig. 3b). The internal angles of a regular polygon with *n* neighbours (Fig. 3c) are given by

$$\theta_n = \frac{n-2}{n} \cdot 180°, \tag{6}$$

and only in few regular configurations, the angles at each vertex will add up to 360° (Fig. 3a). Consider for instance the case of a lattice made of repetitive elements with one square and two octagons: the 90° angle of a square and the 135° angles of two regular octagons (Fig. 3c) add up to 360° at each vertex (Fig. 3a). If in addition, the octagons have about four times the area of the square (Eq. 3), a regular lattice emerges (Fig. 3a, blue). On the contrary, if the areas of neighbouring cells do not match such requirements, irregular lattices emerge (Fig. 3d).

As noted above, in a hexagonal lattice the average number of neighbours is six, i.e., $m_6 = 6 \neq 5 + \frac{8}{6}$ (Fig. 3e, red triangle), which violates Aboav's law (Eq. 4, Fig. 3e, black line), but matches Weaire's law (Eq. 5, Fig. 3e, red line). Also, the other arrangements that result in perfect polygonal lattices (Fig. 3a) deviate from Aboav's law (Eq. 4, black line), but match Weaire's law (Eq. 5, coloured lines) rather well (Fig. 3e). These perfect lattices also all emerge in `LBIBCell` tissue simulations when adhesive circles with the appropriate relative areas are placed at the appropriate relative positions in a grid (Fig. 3a, coloured lattices) and thus represent the configuration with the lowest lateral surface

bioRxiv preprint doi: https://doi.org/10.1101/591461; this version posted March 27, 2019. The copyright holder for this preprint (which was not certified by peer review) is the author/funder, who has granted bioRxiv a license to display the preprint in perpetuity. It is made available under aCC-BY-NC 4.0 International license.

energy. This shows that not all configurations that minimise the lateral contact surface area follow Aboav's law.

In summary, regular polygonal lattices follow Weaire's law more closely than Aboav's law (Fig. 3e), while epithelial tissues follow Aboav's law more closely than Weaire's law (Fig. 2c,d). What is special then about epithelial tissues, and what is the underlying physical principle that leads to these regularities?

The AW law in epithelial tissues

In an epithelial tissue, the apical areas are predetermined by several active processes, including cell growth, cell division, and interkinetic nuclear migration. As a result, the position of cells with a certain area does not follow a pattern that would allow the emergence of a contiguous lattice made from regular polygons. But, why would these lattices follow the AW law?

According to Euler's formula, cells have on average six neighbours [4, 8]. The plot of $m_n \cdot n$ with $m_n = 6$ versus *n* is reasonably close to the AW law (Fig. 4a, black line), but clearly deviates (Fig. 4a, green line). In a contiguous lattice, cells have to meet a further constraint, in that at each vertex point, the combined angle must be 360° (Fig. 3b). At each of the *n* vertices, the neighbouring cells should then have a combined angle of 360° - θ_n (Fig. 4b, inset). The average angle, $\theta_m = \frac{(\theta_1+\theta_2)}{2}$, of the two neighbouring cells therefore follows from $\theta_m = \frac{(360°-\theta_n)}{2} = 180° - \frac{\theta_n}{2} = 180° \cdot \left(1 - \frac{n-2}{2n}\right)$, where we used Eq. 6 for θ_n. We then obtain for the average number of neighbours

$$m_n = \frac{360°}{(180°-\theta_m)} = \frac{4n}{n-2} \ . \qquad (7)$$

bioRxiv preprint doi: https://doi.org/10.1101/591461; this version posted March 27, 2019. The copyright holder for this preprint (which was not certified by peer review) is the author/funder, who has granted bioRxiv a license to display the preprint in perpetuity. It is made available under aCC-BY-NC 4.0 International license.

This relationship approximates the AW law for neighbour numbers close to $n = 5$ rather well, but deviates for larger and smaller neighbour numbers (Fig. 4a, yellow line). We note that the internal angle of regular polygons, θ_n, depends non-linearly on the polygon type n (Eq. 6, Fig. 4b). As a consequence, two cells, whose angles at a vertex add up to $2\theta_m$ yield a different m_n depending on whether their angles are very similar or very different. If we take this non-linear effect into account (see Supplementary Information for details), and integrate within sensible physiological limits, i.e. $\theta_{\min} = 60°$, the smallest internal angle of a regular polygon (triangle), and $\theta_{\max}=\frac{(360°-\theta_{\min})}{2} = 150°$, the internal angle of a regular dodecagon (12-gon), we obtain

$$m_n = \begin{cases} \frac{3n}{(n-3)} \ln\left(5 - \frac{12}{n}\right) & \text{for } 3 < n \leq 12 \\ 2 \ln\left(\frac{10n-24}{n-6}\right) & \text{for } n > 12 \end{cases} , \tag{8}$$

which yields a rather close fit to the AW law for larger n (Fig. 4c, grey line). In the limit of $n \to \infty$, Eq. 8 yields (Fig. 4c, blue line)

$$a = \lim_{n \to \infty} m = \frac{180°}{\theta_{\max} - \theta_{\min}} \ln\left(\frac{180° - \theta_{\min}}{180° - \theta_{\max}} \cdot \frac{\theta_{\max}}{\theta_{\min}}\right) \approx 4.6 , \tag{9}$$

$$b = \lim_{n \to \infty} mn - an = 2\left(\frac{180°}{\theta_{\min}}\right)\left(\frac{180°}{\theta_{\max}}\right) = 7.2 , \tag{10}$$

which is close to the parameters $a = 5$ and $b = 8$ in the AW law as given by Eq. 4 (Fig. 4c, black line), and within the range of parameter values inferred from biological data and the `LBIBCell` simulations (Fig. 2c). Aboav's empirical values $a = 5$ and $b = 8$ are obtained with $\theta_{\min} = 50.4°$ and $\theta_{\max} = 160.7°$, the lower bound of which is plausible only if trigons become distorted.

For small n, Eq. 8 predicts larger values for m_n than what is observed. So, what happens for smaller n? Consider a regular triangle. To meet the angle constraint, it requires neighbouring polygons that

bioRxiv preprint doi: https://doi.org/10.1101/591461; this version posted March 27, 2019. The copyright holder for this preprint (which was not certified by peer review) is the author/funder, who has granted bioRxiv a license to display the preprint in perpetuity. It is made available under aCC-BY-NC 4.0 International license.

each have 12 neighbours (Fig. 3a, purple). To maintain a lattice of equilateral polygons, this would require a tissue with a large variability in cell area (Eq. 3), and a strict pattern of large and small cells (Fig. 3a, purple). Such tissues are unlikely to emerge from biological processes. In the case of more physiological variabilities in apical cell areas, a triangular cell will border cells that have a smaller area than what is required for a regular dodecagon (n=12) according to the quadratic law (Eq. 3). As a consequence, such neighbouring dodecagonal cells would have a smaller side length than the triangular cell. To fit into a contiguous lattice, the polygons would then become stretched and their internal angles would no longer correspond to that of a regular polygon. Alternatively, the neighbours can assume a lower neighbour number than 12. Also in this case, the internal angles can no longer reflect that of a regular polygon as they would no longer add to 360°.

Accordingly, we extended the above formalism to allow for an irregular central polygon that deviates from the perfect internal angle θ_n by an angle θ_i (Fig. 4d, inset; see Supplementary Information for details). In the limit of $n \to \infty$, we recover the same value for the parameter a as for the regular polygon case (Eq. 9), but b now depends also on the maximal value of the deviatory angle θ_i. We obtain an excellent fit to the AW law (a=5, b=8, Fig. 4d, black line) when we use $\theta_\mathrm{min} = 360° - \theta_n - \theta_\mathrm{i} - \theta_\mathrm{max}$ and $\theta_\mathrm{max} = 151.3°$, and set the symmetric upper bounds of the angle mismatch to $|\theta_\mathrm{i}^-| = \theta_\mathrm{i}^+ = 0.59\frac{2\pi}{n}$, where $\frac{2\pi}{n}$ is the upper limit to maintain convexity (Fig. 4d, red line).

In fact, there is sufficient parametric freedom to reproduce all measured values of a and b (Fig. 2c) by adjusting the integration bounds for the angles, θ_min and θ_max, and the upper bounds $\theta_\mathrm{i}^-, \theta_\mathrm{i}^+$ for the angle deviation θ_i. Thus, the neighbour relationships in the *Drosophila* larval wing disc (a=4.76, b=8.34, grey) deviate slightly from the classical AW law (Eq. 4, Fig. 5a, black), but can be reproduced very well by the model (Fig. 5a, red line), and the predicted upper bound, $|\theta_\mathrm{i}^-| = \theta_\mathrm{i}^+ = 0.57\frac{2\pi}{n}$, in the angle deviation matches that observed in the tissue very well (Fig. 5b). Importantly, even though we introduced the irregularity assumption to explain the neighbour relationships of cells with few neighbours, it applies to all polygon types. In agreement with this, the great majority of

bioRxiv preprint doi: https://doi.org/10.1101/591461; this version posted March 27, 2019. The copyright holder for this preprint (which was not certified by peer review) is the author/funder, who has granted bioRxiv a license to display the preprint in perpetuity. It is made available under aCC-BY-NC 4.0 International license.

epithelial cells deviate from a regular shape as measured by their ellipticity, and the irregularity of the apical sides of epithelial cells does not dependent on the cells' neighbour number (Fig. 5c).

Much as the internal angles, we expect the side lengths to deviate from that of a regular polygon. In a regular polygonal lattice, all side lengths should be equal (Eq. 3, Fig. 5d, yellow line), and the average normalised side lengths are indeed close to one (Fig. 5d). Single cells mostly deviate from these averages, much as only the average area per polygon type follows Lewis' law (Eq. 2, Fig. 5e, black line). There are two sources for the observed irregularity. For one, the cellular processes result in a spatial distribution of apical areas in epithelia that are not consistent with the requirements of regular polygonal lattices (Fig. 3a). Secondly, apical areas in epithelia follow a continuous area distribution (Fig. 5f, black line) while the quadratic law (Eq. 3) specifies discrete optimal areas for each polygon type (Fig. 5f, yellow lines). With regard to the second point, we indeed observe that cell shape, side lengths, and angles deviate the least from that of a regular polygon when a cell's neighbour number corresponds to the apical area according to the linear Lewis' law (Eq. 2, Fig. 5g-i, black line) or the quadratic law (Eq. 3, Fig. 5g-i, yellow line).

CONCLUSION

We conclude that the AW law, like Lewis' law, emerges in epithelial tissues because cells minimise the overall lateral surface energy and thus the combined cell perimeter. By following the relationship between polygon area and polygon type as stipulated by Lewis' law (Eq. 2) or the quadratic law (Eq. 3), the difference in side lengths is minimised between cells. By following the neighbour relationships that are described by the phenomenological AW law, the internal angles are closest to that of a regular polygon while adding to 360° at each vertex. Both the linear Lewis' law and the AW law deviate from the curve predicted for a regular polygonal lattice. Regular polygonal lattices, however, require strict patterns of correctly sized cells. Given that cell growth and cell division processes result in a more

bioRxiv preprint doi: https://doi.org/10.1101/591461; this version posted March 27, 2019. The copyright holder for this preprint (which was not certified by peer review) is the author/funder, who has granted bioRxiv a license to display the preprint in perpetuity. It is made available under aCC-BY-NC 4.0 International license.

variable spatial distribution of apical cell sizes, these cannot give rise to a regular polygonal lattice. The observed lattices therefore represent a trade-off to achieve the most regular cell shapes in a contiguous lattice with differently-sized apical areas.

METHODS

Image Processing

Cell boundaries and cell properties (cell area, polygon type, ellipse fit axes) were obtained in (Kokic et al., submitted). In addition, the side lengths and the internal angles of all cells were extracted using EpiTools [5] and the Fiji [17] plugin Tissue Analyzer [18]. To this end, the EpiTools source code was modified to also export the IDs of the n_i neighbours of a cell to permit the calculation of m_n. R scripts were used to extract and analyse data, calculate statistics, and plot the results.

Set-Up of the `LBIBCell` simulations

The `LBIBCell` simulations were set up as described in detail before (Kokic et al, submitted) and is summarised in the Supplementary Material.

Data and Software availability

All source codes are freely available at:

https://git.bsse.ethz.ch/iber/Publications/2019_vetter_kokic_aboav-weaire-law.

Acknowledgements

We thank Davide Heller and Luis M. Escudero for providing access to their raw data. This work has been supported through an SNF Sinergia grant to DI, and grants BFU2012-34324 and BFU2015-66040 (MINECO, Spain) to FC.

bioRxiv preprint doi: https://doi.org/10.1101/591461; this version posted March 27, 2019. The copyright holder for this preprint (which was not certified by peer review) is the author/funder, who has granted bioRxiv a license to display the preprint in perpetuity. It is made available under aCC-BY-NC 4.0 International license.

Author Contributions

DI, RV developed the theoretical framework, MK carried out all image processing, simulations and created all figures, HG, LH, BG contributed preliminary image processing, modelling and data analysis, AI, GV-F, FC contributed the data. DI, RV, FC, MK wrote the manuscript. All authors approved the final manuscript.

REFERENCES:

1. Classen AK, Anderson KI, Marois E, Eaton S. Hexagonal packing of Drosophila wing epithelial cells by the planar cell polarity pathway. Dev Cell. 2005;9(6):805-17. doi: 10.1016/j.devcel.2005.10.016. PubMed PMID: 16326392.
2. Escudero LM, Costa Lda F, Kicheva A, Briscoe J, Freeman M, Babu MM. Epithelial organisation revealed by a network of cellular contacts. Nat Commun. 2011;2:526. doi: 10.1038/ncomms1536. PubMed PMID: 22068593; PubMed Central PMCID: PMCPMC3672852.
3. Farhadifar R, Roper JC, Aigouy B, Eaton S, Julicher F. The influence of cell mechanics, cell-cell interactions, and proliferation on epithelial packing. Curr Biol. 2007;17(24):2095-104. doi: 10.1016/j.cub.2007.11.049. PubMed PMID: 18082406.
4. Gibson MC, Patel AB, Nagpal R, Perrimon N. The emergence of geometric order in proliferating metazoan epithelia. Nature. 2006;442(7106):1038-41. doi: 10.1038/nature05014. PubMed PMID: 16900102.
5. Heller D, Hoppe A, Restrepo S, Gatti L, Tournier AL, Tapon N, et al. EpiTools: An Open-Source Image Analysis Toolkit for Quantifying Epithelial Growth Dynamics. Dev Cell. 2016;36(1):103-16. doi: 10.1016/j.devcel.2015.12.012. PubMed PMID: 26766446; PubMed Central PMCID: PMCPMC4712040.
6. Etournay R, Popovic M, Merkel M, Nandi A, Blasse C, Aigouy B, et al. Interplay of cell dynamics and epithelial tension during morphogenesis of the Drosophila pupal wing. eLife. 2015;4:e07090. doi: 10.7554/eLife.07090. PubMed PMID: 26102528; PubMed Central PMCID: PMCPMC4574473.
7. Sanchez-Gutierrez D, Tozluoglu M, Barry JD, Pascual A, Mao Y, Escudero LM. Fundamental physical cellular constraints drive self-organization of tissues. EMBO J. 2016;35(1):77-88. doi: 10.15252/embj.201592374. PubMed PMID: 26598531; PubMed Central PMCID: PMCPMC4718000.
8. Rivier N, Lissowski A. On the Correlation between Sizes and Shapes of Cells in Epithelial Mosaics. J Phys a-Math Gen. 1982;15(3):L143-L8. doi: Doi 10.1088/0305-4470/15/3/012. PubMed PMID: WOS:A1982NJ24800012.
9. Aboav. The arrangement of grains in polycrystals. Metallography. 1970;3:383-90.
10. Jeune B, Barabé D. The Use of the Aboav-Weaire Law to Estimate a Biological Constraint. Journal of Biological Systems. 2002;10(01):33-45. doi: 10.1142/s0218339002000482.
11. Mombach JCM, de Almeida RMC, Iglesias JR. Two-cell correlations in biological tissues. Phys Rev E. 1993;47(5):3712-6. doi: 10.1103/PhysRevE.47.3712.

bioRxiv preprint doi: https://doi.org/10.1101/591461; this version posted March 27, 2019. The copyright holder for this preprint (which was not certified by peer review) is the author/funder, who has granted bioRxiv a license to display the preprint in perpetuity. It is made available under aCC-BY-NC 4.0 International license.

12. Mombach JCM, Vasconcellos MAZ, Almeida RMCd. Arrangement of cells in vegetable tissues. Journal of Physics D: Applied Physics. 1990;23(5):600-6. doi: 10.1088/0022-3727/23/5/021.

13. Weaire D. Some Remarks on the Arrangement of Grains in a Polycrystal. Metallography. 1974;7:157-60.

14. Chiu SN. Aboav-Weare's and Lewis' Laws-A Review. MATERIALS CHARACTERIZATION. 1995;34:149-65.

15. Tanaka S, Sichau D, Iber D. LBIBCell: a cell-based simulation environment for morphogenetic problems. Bioinformatics. 2015;31(14):2340-7. doi: 10.1093/bioinformatics/btv147. PubMed PMID: 25770313.

16. Hertwig O. Das Problem der Befruchtung und der Isotropie des Eies. Eine Theorie der Vererbung. Jenaische Zeitschrift für Naturwissenschaft. 1884;18:274.

17. Schindelin J, Arganda-Carreras I, Frise E, Kaynig V, Longair M, Pietzsch T, et al. Fiji: an open-source platform for biological-image analysis. Nat Methods. 2012;9(7):676-82. doi: 10.1038/nmeth.2019. PubMed PMID: 22743772; PubMed Central PMCID: PMCPMC3855844.

18. Aigouy B, Umetsu D, Eaton S. Segmentation and Quantitative Analysis of Epithelial Tissues. Drosophila: Methods and Protocols, 2nd Edition. 2016;1478:227-39. doi: 10.1007/978-1-4939-6371-3_13. PubMed PMID: WOS:000400686500014.

19. Aegerter-Wilmsen T, Smith AC, Christen AJ, Aegerter CM, Hafen E, Basler K. Exploring the effects of mechanical feedback on epithelial topology. Development. 2010;137(3):499-506. doi: 10.1242/dev.041731. PubMed PMID: 20081194.

bioRxiv preprint doi: https://doi.org/10.1101/591461; this version posted March 27, 2019. The copyright holder for this preprint (which was not certified by peer review) is the author/funder, who has granted bioRxiv a license to display the preprint in perpetuity. It is made available under aCC-BY-NC 4.0 International license.

Figure legends

Figure 1: Principles of Epithelial Organisation

(a) A cartoon of an epithelial tissue. The tissue is polarized with an apical and basal side. At the apical side cells adhere tightly via adhesion junctions (green). Nuclei are depicted in pink.

(b) The epithelial cells (denoted as faces - *f*) form a contiguous polygonal lattice on the apical side. Typically, three edges, *e*, meet in a vertex, *v*.

(c) Tissues differ widely in the frequency of neighbour numbers. The legend provides the measured average number of cell neighbours for each tissue and the references to the primary data [1-7]. Data points for $n < 3$ were removed as they must present segmentation artefacts. The tissue samples are: Chick neural tube epithelium (cNT) [2], *Drosophila* eye disc (EYE) [2], *Drosophila* peripodal membrane from the larval eye disc (dPE), *Drosophila* larval wing disc (dWL) [1-6, 19] (Kokic et al, submitted), *Drosophila* pre-pupal wing disc (dWP) [1, 2], *Drosophila* mutant wing pre-pupa (dMWP: the expression of myosin II was reduced in the wing disc epithelium by expressing an UAS-zipper-RNAi using the C765-Gal4 line) [2], and *Drosophila* pupal wing disc (dPW) [1]. In case of the *Drosophila* peripodal membrane from the larval eye disc (dPE), the numbers indicate the developmental age as the number of ommatidial rows that have formed. In case of the *Drosophila* pupal wing disc (dPW) [2], TPx indicates subsequent, but not further specified pupal time points [1]; 30h and 48h specifies the time post puparium formation.

(d) The measured average number of cell neighbours is close to the topological requirement $\bar{n} = 6$ in all tissues; see panel c for the colour code.

(e) The relative average cell area, $\frac{\overline{A_n}}{\bar{A}}$, is linearly related to the number of neighbours, *n*, and follows Lewis' law (Eq. 2, black line) in all reported tissues. The colour code is as in panel c, but data is available only for a subset of those tissues. Few cells with more than 7 neighbours have been measured and estimates of the mean areas are therefore unreliable (shaded part).

(f) The normalised side length of a regular polygon with *n* vertices for a fixed area.

bioRxiv preprint doi: https://doi.org/10.1101/591461; this version posted March 27, 2019. The copyright holder for this preprint (which was not certified by peer review) is the author/funder, who has granted bioRxiv a license to display the preprint in perpetuity. It is made available under aCC-BY-NC 4.0 International license.

(g) The AW law formulates a relationship between the number of neighbours, n, that a cell has and the average number of neighbours, m_n, that its direct neighbours have. The product $m_n \cdot n$ can be determined by summing over all n neighbours.

(h) The epithelial tissues follow the AW law (black line). The colour code is as in panel c, but data is available only for a subset of those tissues.

Panels a-f are reproduced with modifications from (Kokic et al, submitted).

Figure 2: The AW law emerges in `LBIBCell` Simulations

(a) Representation of the apical epithelial surface as a 2D simulation plane in LBIBCell. The cartoon shows a cubical section of a simple columnar pseudostratified epithelium. LBIBCell simulates the tissue mechanics and morphodynamics of the 2D plane (indicated in pink) that goes through the adherens junctions (marked in green), which are located below the apical surface. Cell boundaries are geometrically highly resolved and cell boundaries and cell-cell junctions are modelled with elastic springs. The cartoon and legend are reproduced with modifications from (Kokic et al, submitted).

(b) The AW law plotted for `LBIBCell` simulations with random cell division (blue) or cell division perpendicular to the longest axis (red).

(c) The estimated coefficients a, b when fitting $m_n \cdot n = a \cdot n + b$ to the data (Fig. 1h) and the `LBIBCell` simulations (Fig. 2b).

(d) The estimated coefficient b when fitting $m_n \cdot n = a \cdot n + b$ does not positively correlate with $6 + Var(n)$ in epithelia. ρ is the Pearson correlation coefficient.

(e) The hexagon fraction versus the variance in the polygon distribution $Var(n)$ for all available data.

Figure 3: The AW law does not emerge in perfect lattices

(a) In case of appropriate relative sizes and positions, adherence of circles results in perfect lattices (grey), as confirmed in `LBIBCell` simulations.

bioRxiv preprint doi: https://doi.org/10.1101/591461; this version posted March 27, 2019. The copyright holder for this preprint (which was not certified by peer review) is the author/funder, who has granted bioRxiv a license to display the preprint in perpetuity. It is made available under aCC-BY-NC 4.0 International license.

(b) The angles at each tricellular junction have to add up to 360°.

(c) Interior angles of regular polygons.

(d) In case of inappropriate relative sizes and positions, adherence between circles results in imperfect lattices.

(e) The products of $m_n \cdot n$ versus neighbour number n for the perfect lattices in panel a deviate from Aboav's law (Eq. 4, black line), but match Weaire's law (Eq. 5, coloured lines; colour code as in panel a) rather well. Results from `LBIBCell` simulations (triangles) are close to analytic results (circles).

Figure 4: The AW law in epithelial tissues arises because of an angle constraint.

(a) The product of $m_n \cdot n$ versus neighbour number n for the AW law (black), $m_n = 6$ (green), $m_n = \frac{4n}{n-2}$ (yellow).

(b) Interpolation between the angles of regular polygons, $\theta_n = \frac{n-2}{n} \cdot 180°$, versus the number of vertices *n*. *Inset:* A cartoon of the angles at a tricellular junction between a cell with *n* neighbours and its two neighbours with angles θ_1 and θ_2.

(c) Comparison of an analytical approximation for regular polygons (Eq. 8, grey) and its asymptote ($a \approx 4.6$ and $b = 7.2$) (blue) to Aboav–Weaire's law (black).

(d) Comparison of an analytical approximation for irregular polygons (red) to Aboav–Weaire's law (black). *Inset:* A cartoon of the angles at a tricellular junction in case of an irregular central polygon with angle $\theta_n + \theta_\mathrm{i}$.

Figure 5: Individual apical areas in epithelia are irregular.

(a) The product of $m_n \cdot n$ versus neighbour number n for cells in the *Drosophila* wing disc follows the AW law on average (black line), and is approximated very well by the analytical approximation for irregular polygons (red line) when optimizing the angle bounds $\left(\theta_\mathrm{min} = 360° - \theta_n - \theta_\mathrm{i} -\right.$

bioRxiv preprint doi: https://doi.org/10.1101/591461; this version posted March 27, 2019. The copyright holder for this preprint (which was not certified by peer review) is the author/funder, who has granted bioRxiv a license to display the preprint in perpetuity. It is made available under aCC-BY-NC 4.0 International license.

$\theta_{\max}, \theta_{\max} = 151.3°, |\theta_{\mathrm{i}}^{-}| = \theta_{\mathrm{i}}^{+} = 0.59\frac{2\pi}{n}\Big)$ to match the AW law (a=4.76, b=8.34) that best matches the data (Fig. 2c).

(b) Angle versus polygon type for cells in the *Drosophila* wing disc. The observed average angles are those of regular polygons (yellow lines). The red solid lines mark $\theta_n \pm \theta_{\mathrm{i}}^{+}$, the predicted angle range of the irregular central polygon with $\theta_{\mathrm{i}}^{+} = 0.59\frac{2\pi}{n}$.

(c) Ellipticity of cells in the *Drosophila* wing disc as measured by the ratio of the axes of fitted ellipses. A ratio of 1 (yellow line) corresponds to regular polygons.

(d) Normalised side length versus polygon type for cells in the *Drosophila* wing disc. The mean deviates from the ideal curve $\frac{\overline{S_n}}{\bar{S}} = 1$ (yellow line).

(e) The relative average cell area, $\frac{\overline{A_n}}{\bar{A}}$, for cells in the *Drosophila* wing disc. The average is linearly related to the number of neighbours, n, in the *Drosophila* wing disc, and follows the linear Lewis' law (Eq. 2, black line) rather than the quadratic law (Eq. 3, yellow line).

(f) Normalised area distribution for cells in the *Drosophila* wing disc. The yellow vertical lines mark the areas for each polygon type required to form a regular polygon lattice (Eq. 3).

(g-i) Ellipticity, as measured by the ratio of the axes of fitted ellipses, (f), variation of side length (g), and variation in the angles (h) of single cells in the *Drosophila* wing disc versus the fold-deviation of their apical area, A_i, from that appropriate for their polygon type, $\overline{A_n}$, according to either the linear Lewis' law (Eq. 2, black line) or the quadratic law (Eq. 3, yellow line). Variability in side length and angles was calculated for each cell as $\frac{x_j - <x>}{<x>}$, where x_j refers to side length or angle, respectively, of each cell j, and $< x >$ indicates the expected value for the particular polygon type of the cell.

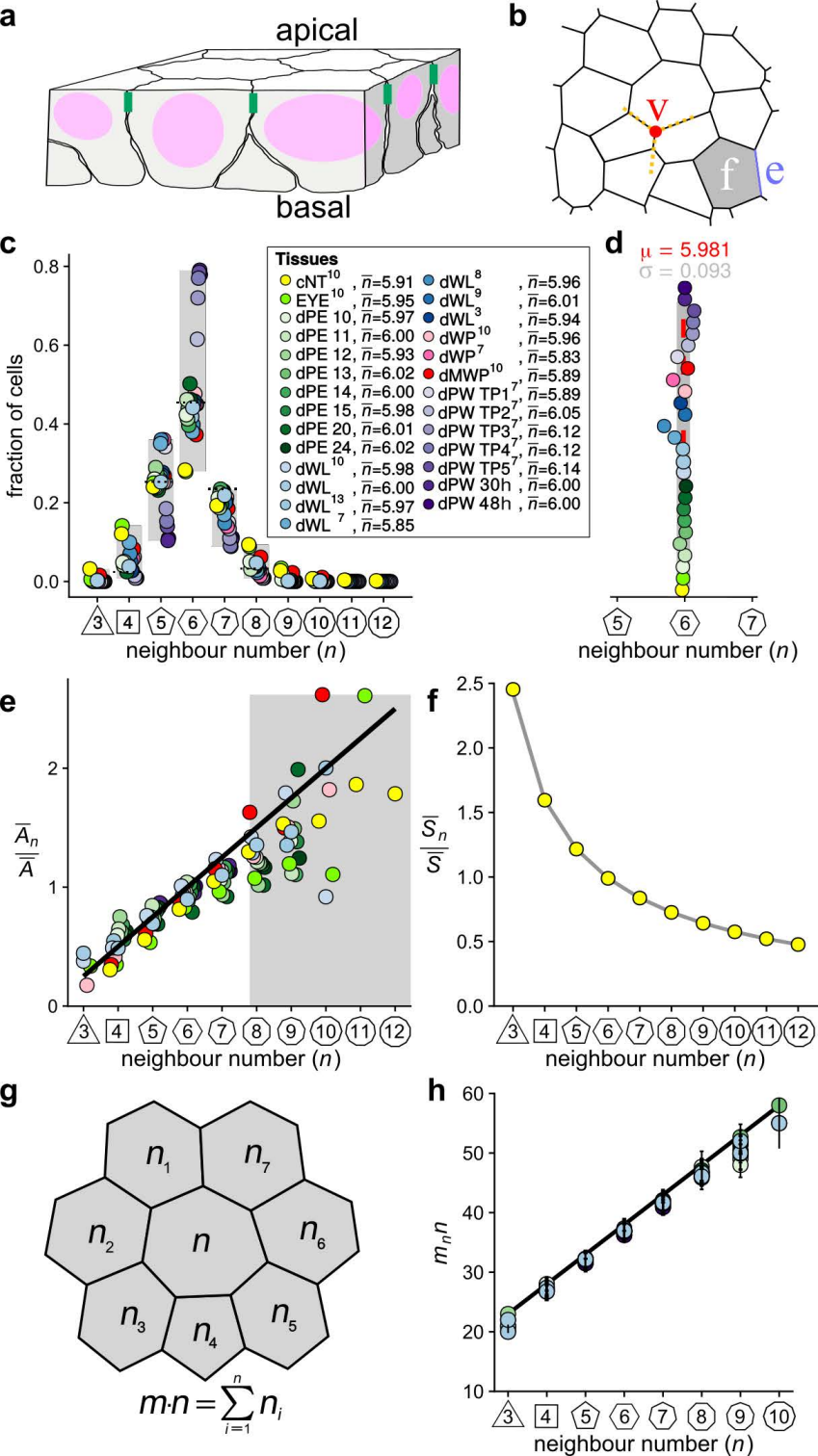
a
apical
basal
b
V
f
e
c
fraction of cells
neighbour number (n)
Tissues
cNT10, n̄=5.91
EYE10, n̄=5.95
dPE 10, n̄=5.97
dPE 11, n̄=6.00
dPE 12, n̄=5.93
dPE 13, n̄=6.02
dPE 14, n̄=6.00
dPE 15, n̄=5.98
dPE 20, n̄=6.01
dPE 24, n̄=6.02
dWL10, n̄=5.98
dWL, n̄=6.00
dWL13, n̄=5.97
dWL7, n̄=5.85
dWL8, n̄=5.96
dWL9, n̄=6.01
dWL3, n̄=5.94
dWP10, n̄=5.96
dWP7, n̄=5.83
dMWP10, n̄=5.89
dPW TP17, n̄=5.89
dPW TP27, n̄=6.05
dPW TP37, n̄=6.12
dPW TP47, n̄=6.12
dPW TP57, n̄=6.14
dPW 30h, n̄=6.00
dPW 48h, n̄=6.00
d
μ = 5.981
σ = 0.093
neighbour number (n)
e
neighbour number (n)
f
neighbour number (n)
g
n1
n7
n2
n
n6
n3
n4
n5
m·n = Σ_{i=1}^{n} n_i
h
m_n n
neighbour number (n)

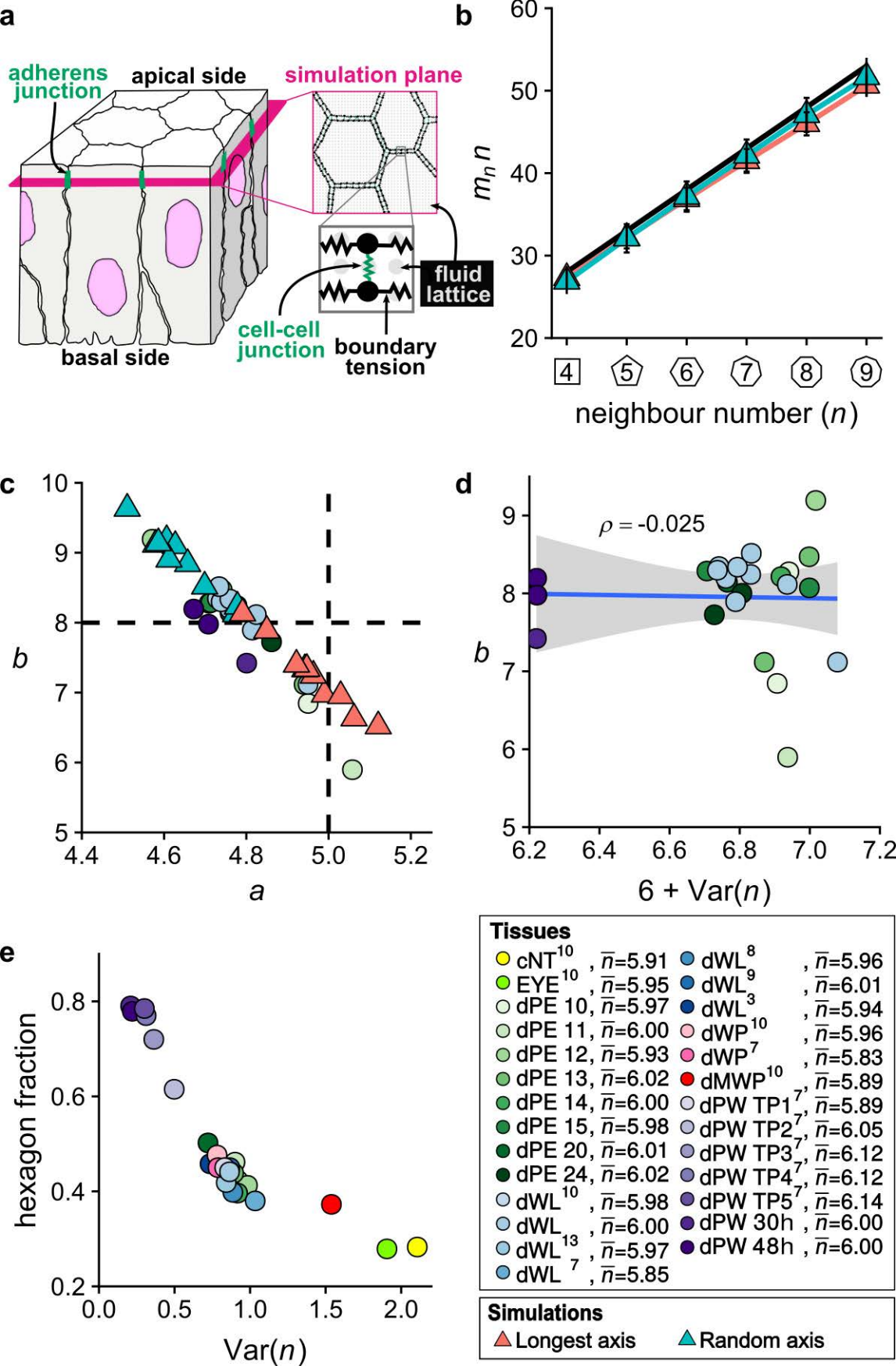
a
adherens junction
apical side
simulation plane
fluid lattice
cell-cell junction
boundary tension
basal side
b
$m_n n$
neighbour number (n)
c
b
a
d
ρ = -0.025
b
6 + Var(n)
e
hexagon fraction
Var(n)
Tissues
cNT10, $\bar{n}$=5.91
EYE10, $\bar{n}$=5.95
dPE 10, $\bar{n}$=5.97
dPE 11, $\bar{n}$=6.00
dPE 12, $\bar{n}$=5.93
dPE 13, $\bar{n}$=6.02
dPE 14, $\bar{n}$=6.00
dPE 15, $\bar{n}$=5.98
dPE 20, $\bar{n}$=6.01
dPE 24, $\bar{n}$=6.02
dWL10, $\bar{n}$=5.98
dWL, $\bar{n}$=6.00
dWL13, $\bar{n}$=5.97
dWL7, $\bar{n}$=5.85
dWL8, $\bar{n}$=5.96
dWL9, $\bar{n}$=6.01
dWL3, $\bar{n}$=5.94
dWP10, $\bar{n}$=5.96
dWP7, $\bar{n}$=5.83
dMWP10, $\bar{n}$=5.89
dPW TP17, $\bar{n}$=5.89
dPW TP27, $\bar{n}$=6.05
dPW TP37, $\bar{n}$=6.12
dPW TP47, $\bar{n}$=6.12
dPW TP57, $\bar{n}$=6.14
dPW 30h, $\bar{n}$=6.00
dPW 48h, $\bar{n}$=6.00
Simulations
Longest axis
Random axis

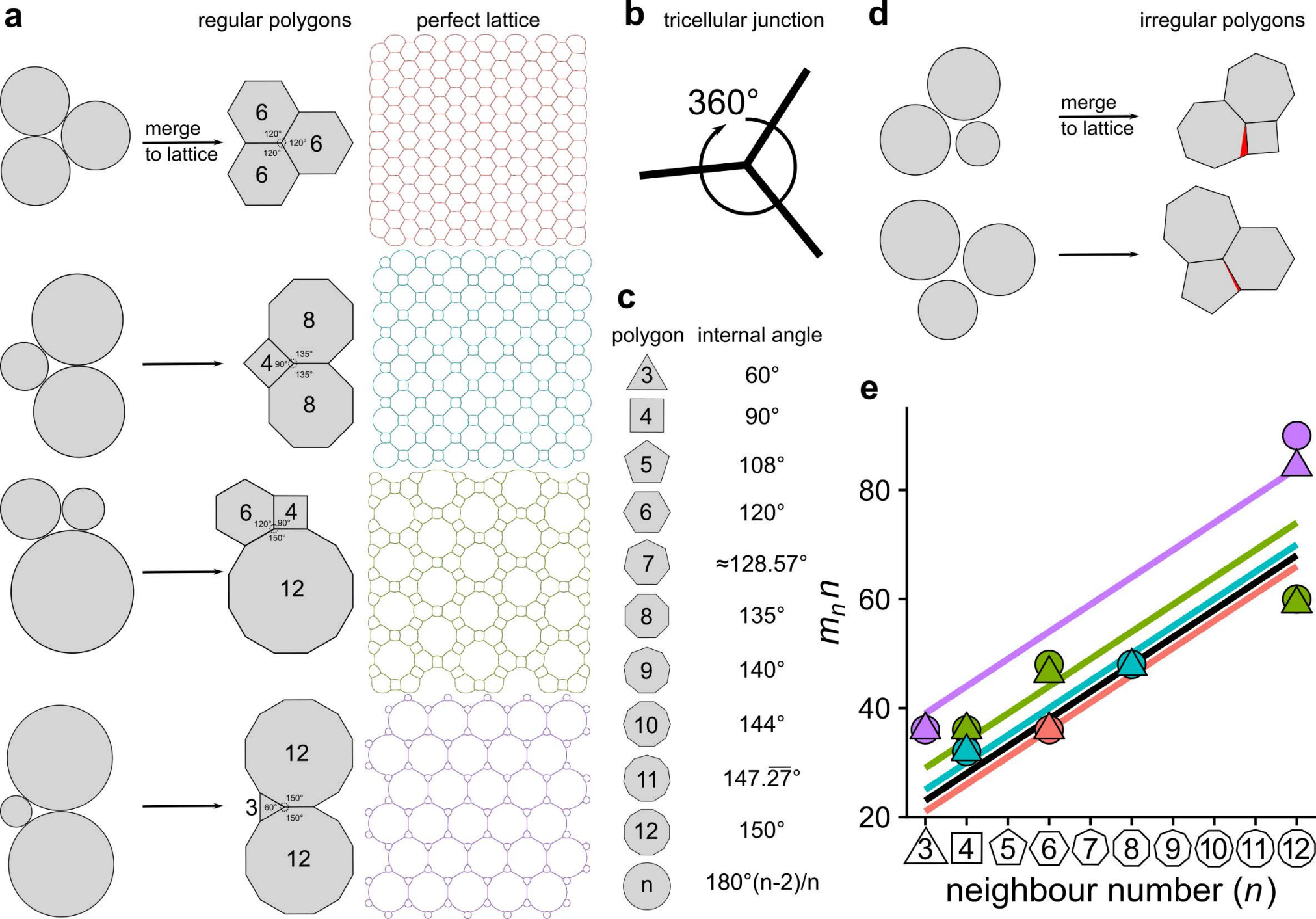
a
regular polygons
perfect lattice
merge
to lattice
6
120°
120°
120°
6
6
8
135°
4
90°
135°
8
6
4
120°
90°
150°
12
12
3
60°
150°
150°
12
b
tricellular junction
360°
c
polygon
internal angle
3
60°
4
90°
5
108°
6
120°
7
≈128.57°
8
135°
9
140°
10
144°
11
147.27°
12
150°
n
180°(n-2)/n
d
irregular polygons
merge
to lattice
e
$m_n n$
80
60
40
20
3
4
5
6
7
8
9
10
11
12
neighbour number (n)

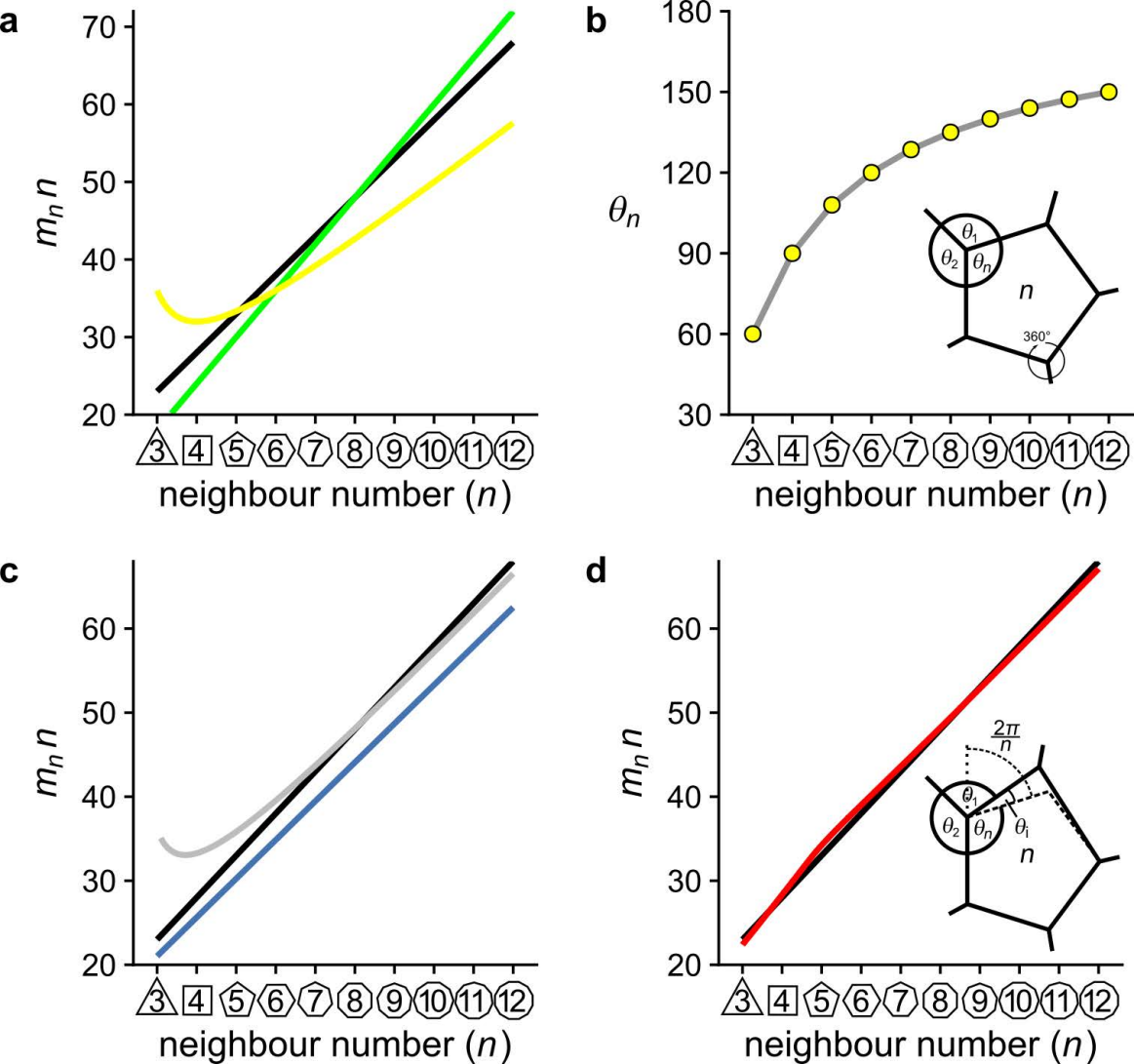
a
b
c
d
$m_n n$
θ_n
neighbour number (n)
θ_1
θ_2
θ_n
n
360°
$\frac{2\pi}{n}$
θ_i

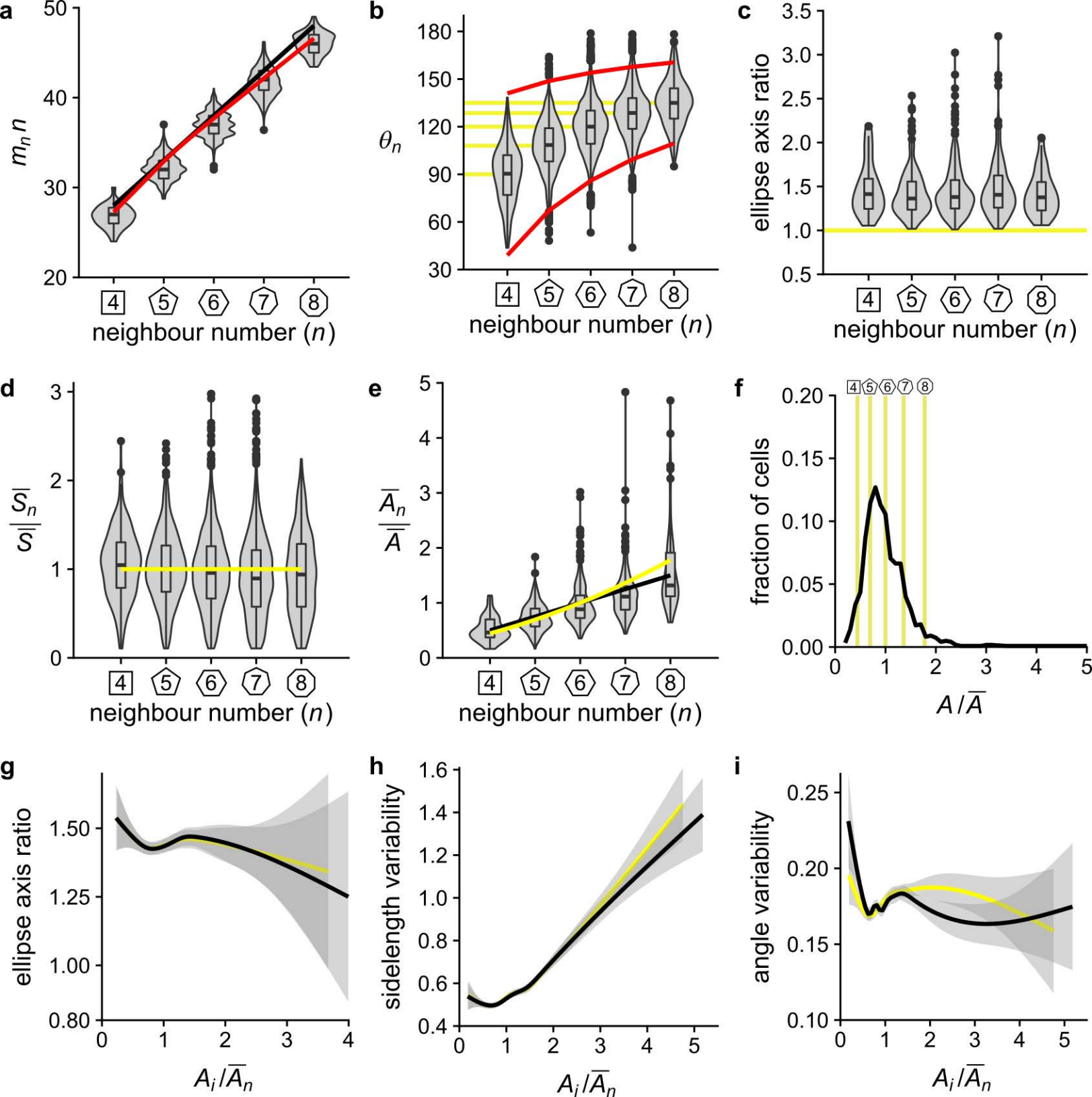
a
$m_n n$
neighbour number (n)
b
θ_n
neighbour number (n)
c
ellipse axis ratio
neighbour number (n)
d
$\frac{S_n}{\overline{S}}$
neighbour number (n)
e
$\frac{\overline{A}_n}{\overline{A}}$
neighbour number (n)
f
fraction of cells
$A/\overline{A}$
g
ellipse axis ratio
$A_i/\overline{A}_n$
h
sidelength variability
$A_i/\overline{A}_n$
i
angle variability
$A_i/\overline{A}_n$

Aboave-Weaire's law in epithelia results from an angle constraint in contiguous polygonal lattices - Supplementary Material

Roman Vetter[1,2,†], Marco Kokic[1,2,†], Harold Gómez[1,2], Leonie Hodel[1], Bruno Gjeta[1], Antonella Iannini[3], Gema Villa-Fombuena[3], Fernando Casares[3], and Dagmar Iber[1,2,‡]

[1]Department of Biosystems, Science and Engineering (D-BSSE), ETH Zurich, Mattenstrasse 26, 4058 Basel, Switzerland
[2]Swiss Institute of Bioinformatics (SIB), Mattenstrasse 26, 4058 Basel, Switzerland
[3]CABD, Universidad Pablo de Olavide, Seville, Spain
[†]The authors contributed equally.
[‡]Corresponding author: Dagmar Iber - dagmar.iber@bsse.ethz.ch

Contents

1 Analytical approximation to Aboav–Weaire's law **2**
1.1 Approximation for regular polygons 2
1.2 Generalisation to irregular polygons 6

2 `LBIBCell` Simulations **9**

3 Supplementary Tables **10**

1 Analytical approximation to Aboav–Weaire's law

1.1 Approximation for regular polygons

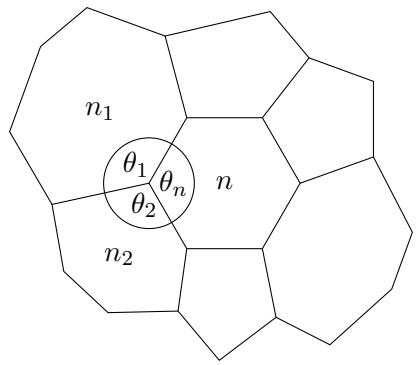

Figure S1: Illustration of a cell neighbourhood with regular central cell.

Consider the case of a regular polygon with n edges in the centre of a local epithelial cell neighbourhood. The interior angles of a regular polygon are given by

$$\theta_n = \pi \frac{n-2}{n}. \tag{1}$$

Inversely, the number of edges can be obtained from the interior angles as

$$n = \frac{2\pi}{\pi - \theta_n}. \tag{2}$$

Assuming that all junctions are tri-cellular as illustrated in Fig. S1, and given θ_n, the average angle left for the two neighbouring cells is

$$\theta_m = \frac{\theta_1 + \theta_2}{2} = \frac{2\pi - \theta_n}{2} \tag{3}$$

at each vertex. If $\theta_1 = \theta_2$ and also both neighbour cells are regular polygons, the mean neighbour number of all neighbours of a cell with n neighbours follows as

$$m_n = \frac{2\pi}{\pi - \theta_m} = \frac{4n}{n-2}. \tag{4}$$

However, in most polygonal lattices, θ_1 and θ_2 differ. We are therefore now averaging over all allowed values of θ_1:

$$m_n = \left\langle \frac{n_1 + n_2}{2} \right\rangle_{\theta_1} \tag{5}$$

where

$$n_1 = \frac{2\pi}{\pi - \theta_1}, \qquad n_2 = \frac{2\pi}{\pi - \theta_2} \tag{6}$$

with

$$\theta_2 = 2\pi - \theta_n - \theta_1. \tag{7}$$

The average is taken over a physiological range $[\theta_{\min}, \theta_{\max}]$ (to be specified later):

$$m_n = \left\langle \frac{\pi}{\pi - \theta_1} + \frac{\pi}{\pi - \theta_2} \right\rangle_{\theta_1} = \frac{1}{\theta_{\max} - \theta_{\min}} \int_{\theta_{\min}}^{\theta_{\max}} \frac{\pi \theta_n}{(\pi - \theta_1)(\pi - \theta_2)} \, \mathrm{d}\theta_1. \tag{8}$$

Notice that this definition is symmetric in θ_1, θ_2, i.e., one could also average over θ_2 instead. The integral in Eq. 8 can be cast into the form

$$\int \frac{1}{A\theta^2 + B\theta + C}\,\mathrm{d}\theta \tag{9}$$

with coefficients

$$A = -\frac{1}{\pi}, \qquad B = 2 - \frac{\theta_n}{\pi} = \frac{n+2}{n}, \qquad C = \theta_n - \pi = -\frac{2\pi}{n}, \tag{10}$$

which evaluates to

$$\int \frac{1}{A\theta^2 + B\theta + C}\,\mathrm{d}\theta = \frac{1}{\sqrt{-D}} \ln\left|\frac{2A\theta + B - \sqrt{-D}}{2A\theta + B + \sqrt{-D}}\right| + \text{const}, \tag{11}$$

where

$$D = 4AC - B^2 = -\left(\frac{n-2}{n}\right)^2 < 0. \tag{12}$$

Therefore, after some basic algebra, Eq. 8 can be evaluated to

$$m_n = \frac{\pi}{\theta_{\max} - \theta_{\min}} \ln\left|\frac{\pi - \theta_{\min}}{\pi - \theta_{\max}}\,\frac{\theta_n - (\pi - \theta_{\max})}{\theta_n - (\pi - \theta_{\min})}\right|. \tag{13}$$

Eq. 13 requires careful selection of the integration bounds $\theta_{\min}$, $\theta_{\max}$, which can be functions of n in general. Trigons are the polygons with the lowest possible neighbour number, and assuming regular polygons, a consistent choice for the minimum allowable angle is

$$\underline{\theta} = \frac{\pi}{3}. \tag{14}$$

For the upper bound, a natural choice appears to be

$$\overline{\theta} = \frac{2\pi - \underline{\theta}}{2} = \frac{5}{6}\pi \tag{15}$$

(corresponding to $n = 12$), as cells with more than 12 edges are hardly ever observable in epithelial tissue. Since this rationale applies to both angles θ_1 and θ_2 alike, and since they are coupled via Eq. 7, the bounds must be applied symmetrically, yielding

$$\begin{aligned} \theta_{\min} &= \max\left\{\underline{\theta},\, 2\pi - \theta_n - \overline{\theta}\right\} \\ \theta_{\max} &= \min\left\{\overline{\theta},\, 2\pi - \theta_n - \underline{\theta}\right\}. \end{aligned} \tag{16}$$

As long as $n \leq 12$, this evaluates to $\theta_{\min} = 7\pi/6 - \theta_n$ and $\theta_{\max} = 5\pi/6$ (Fig. S2). With these integration bounds, Eq. 13 becomes

$$m_n = \begin{cases} \dfrac{3n}{n-3} \ln\left[5 - \dfrac{12}{n}\right] & \text{for } 3 < n \leq 12 \\ 2\ln\left[\dfrac{10n - 24}{n-6}\right] & \text{for } n \geq 12 \end{cases}. \tag{17}$$

This relationship approximates Aboav–Weaire's empirical law very well for $n \geq 6$ (Fig. S3). Aboav–Weaire's law can thus be explained for large n by the cell's tendency toward a regular shape under the constraint that the three angles at cell junctions must sum up to 2π.

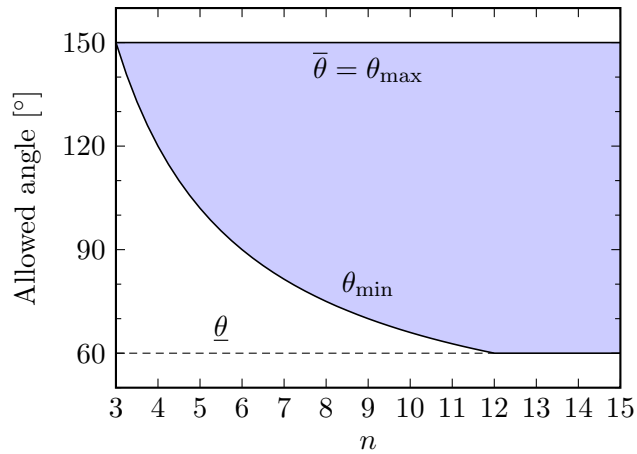

Figure S2: Integration bounds as defined in Eq. 16. The blue region indicates the integration domain.

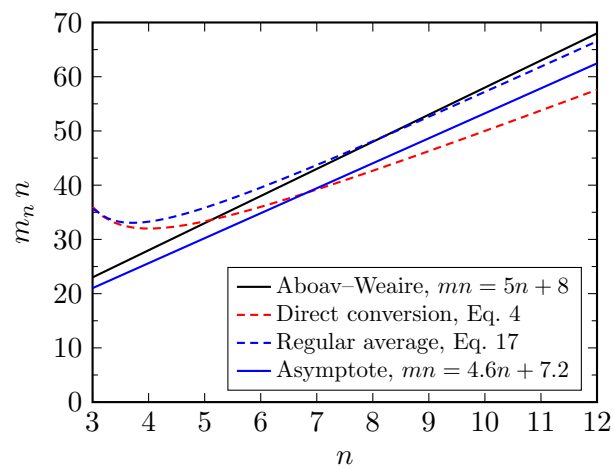

Figure S3: Comparison of analytical approximations to Aboav–Weaire's law for regular polygons.

We now consider the asymptotic behavior in the limit of large n. Aboav's empirical law reads

$$mn = an + b \tag{18}$$

with coefficients $a = 5$, $b = 8$ originally observed in polycrystals [1]. Weaire derived the coefficients $a = 5$, $b = 6$ under a mean field approximation of polygonal regularity, which led him to suggest that $b = 6 + \mathrm{Var}(n)$ [17]. Taking the limit in Eq. 13, we find a linear asymptote with

$$a = \lim_{n\to\infty} m_n = \frac{\pi}{\theta_{\max} - \theta_{\min}} \ln\left[\frac{\pi - \theta_{\min}}{\pi - \theta_{\max}} \frac{\theta_{\max}}{\theta_{\min}}\right] = 2\ln 10 \approx 4.605... \tag{19}$$

and

$$b = \lim_{n\to\infty} mn - an = 2\left(\frac{\pi}{\theta_{\min}}\right)\left(\frac{\pi}{\theta_{\max}}\right) = \frac{36}{5} = 7.2. \tag{20}$$

Both of these values lie remarkably well within the experimentally observed range of the coefficients for epithelial tissue (see Fig. 2c in the main article). Other values can be obtained if the physiological range over which the average is taken is chosen differently. The dependence of a and

b on the integration bounds is shown in Fig. S4 along with the inverse relationship. As an example, Aboav's empirical values $a = 5$, $b = 8$ are obtained if $\theta_{\min} \approx 50.4°$ and $\theta_{\max} \approx 160.7°$, which are physiologically plausible values for epithelial tissue. Taking the mean epithelial coefficients $a = 4.8$, $b = 8$ (Fig. 2c) as a reference, we find the slightly tighter bounds $\theta_{\min} \approx 51.9°$ and $\theta_{\max} \approx 156.0°$.

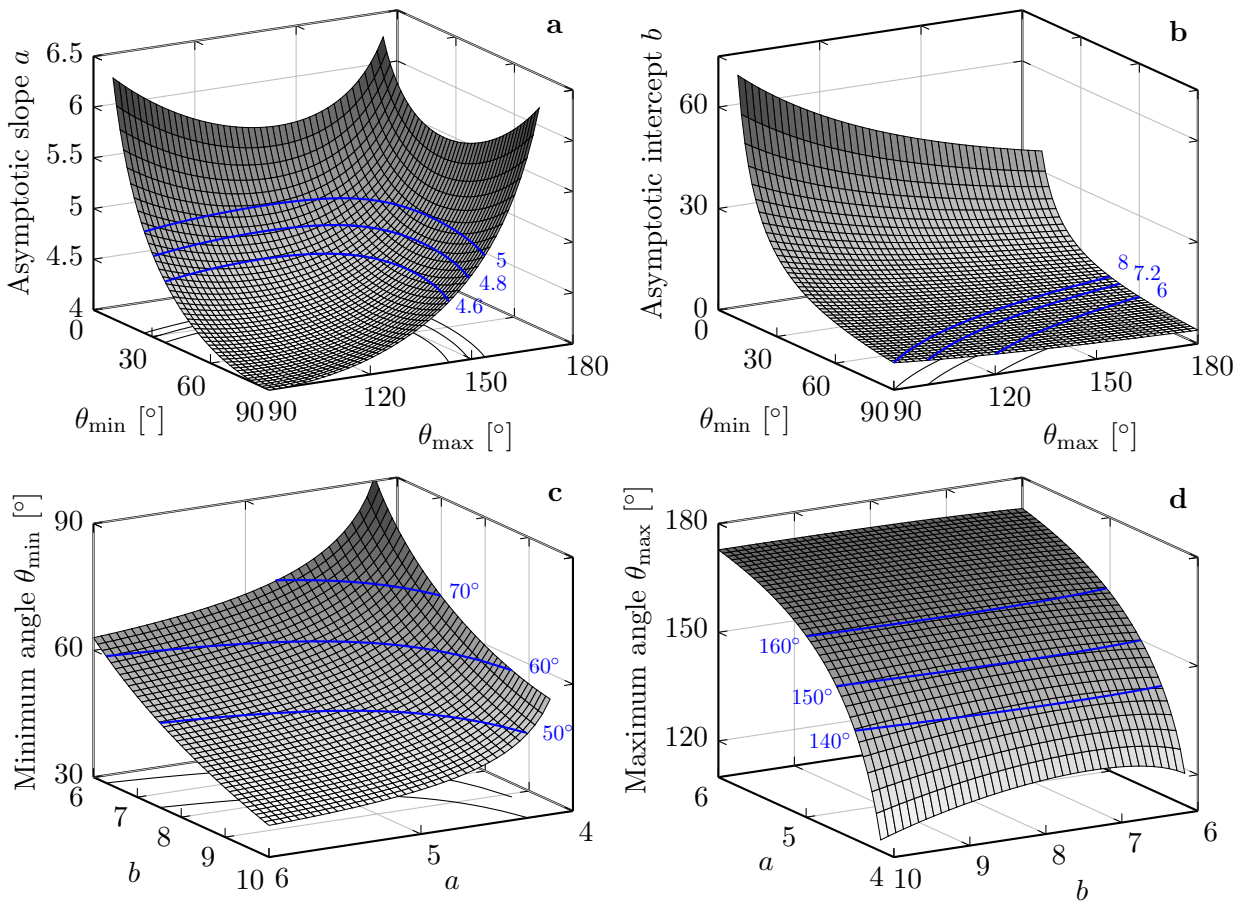

Figure S4: Asymptotic behavior of the analytical approximation in the limit $n \to \infty$. (a-b) Line coefficients a and b as a function of the integration bounds $\theta_{\min}$ and $\theta_{\max}$. Typical values for a and b are highlighted as blue contour lines. Aboav–Weaire's linear law can be obtained asymptotically by intersecting the contours for the desired values of a and b, yielding the physiological range for the angles. (c-d) Inverse relationship, obtained by numerical inversion of Eqs. 19 and 20.

1.2 Generalisation to irregular polygons

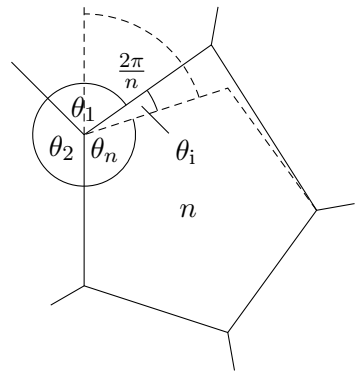

Figure S5: Illustration of the neighbourhood of an irregular polygon. The internal angle deviates from that of a regular polygon, θ_n, by the angle θ_i. The dashed lines mark the outline of a regular pentagon in the centre, as well as the maximal angle $\theta_\mathrm{i}^+ < \frac{2\pi}{n}$ for θ_i to maintain convexity. The angles of the three polygons, $\theta_\mathrm{n} + \theta_\mathrm{i}$, θ_1, θ_2, must add to 2π.

Evidently, the regularity assumption on the polygonal cell shape breaks down for small n. Eq. 17 predicts higher polygon types around triangles, quadrilaterals and pentagons than can be observed in many cellular arrangements (Fig. S3). In real epithelial tissue, cells with large area are not available discretionarily, as required for the regularity assumption to hold for small n. Additionally, side lengths between neighbouring cells must match at shared edges, posing further limitations on the attainable cell regularity in a contiguous lattice. Therefore, a generalisation of the above formalism is proposed here for irregular central polygons.

We now consider a deviation θ_i from the internal angle of a regular polygon (Eq. 1) (Fig. S5), and calculate the expected neighbour number of direct neighbours by averaging over a physiological range $\theta_\mathrm{i} \in [\theta_\mathrm{i}^-, \theta_\mathrm{i}^+]$, yielding

$$m_n = \frac{1}{\mathrm{Vol}(I)} \int_I \frac{1}{\theta_\mathrm{max} - \theta_\mathrm{min}} \int_{\theta_\mathrm{min}}^{\theta_\mathrm{max}} \frac{\pi}{(\pi - \theta_1)} + \frac{\pi}{(\pi - \theta_2)} \, \mathrm{d}\theta_1 \, \mathrm{d}\theta_\mathrm{i} \tag{21}$$

subject to the modified angle sum constraint

$$\theta_2 = 2\pi - \theta_n - \theta_\mathrm{i} - \theta_1 \tag{22}$$

and modified integration bounds

$$\begin{aligned} \theta_\mathrm{min} &= \max\left\{\underline{\theta},\, 2\pi - \theta_n - \theta_\mathrm{i} - \overline{\theta}\right\} \\ \theta_\mathrm{max} &= \min\left\{\overline{\theta},\, 2\pi - \theta_n - \theta_\mathrm{i} - \underline{\theta}\right\}. \end{aligned} \tag{23}$$

Here, I denotes the set of possible irregularity angles

$$I = \left\{\theta_\mathrm{i} \mid \theta_\mathrm{min} < \theta_\mathrm{max},\, \theta_\mathrm{i}^- \leq \theta_\mathrm{i} \leq \theta_\mathrm{i}^+\right\} \tag{24}$$

which depends on n through Eqs. 23 and 1, and

$$\mathrm{Vol}(I) = \int_I \mathrm{d}\theta_\mathrm{i} \tag{25}$$

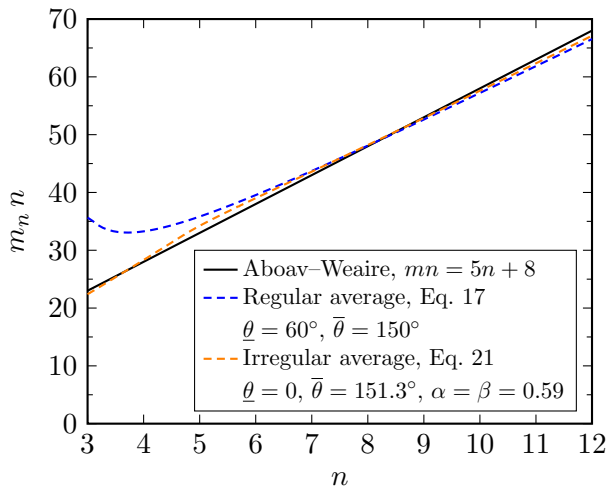

Figure S6: Comparison of analytical approximations to Aboav–Weaire's law for irregular polygons.

is its volume (in the present one-dimensional case, its length). A natural choice for the permitted degree of irregularity appears to be to set the bounds θ_i^-, θ_i^+ to a certain fraction of the turning angle of regular polygons, $\pi - \theta_n = 2\pi/n$, which represents the maximum excess angle that will maintain convexity of the polygon (Fig. S5). It is therefore reasonable to set

$$\theta_\mathrm{i}^- = -\alpha\frac{2\pi}{n}, \qquad \theta_\mathrm{i}^+ = \beta\frac{2\pi}{n} \tag{26}$$

with free (but possibly interrelated) coefficients $\alpha, \beta \in [0, 1)$.

The inner integral in Eq. 21 can be evaluated using Eq. 13, yielding

$$m_n = \frac{1}{\mathrm{Vol}(I)} \int_I \frac{\pi}{\theta_\mathrm{max} - \theta_\mathrm{min}} \ln\left|\frac{\pi - \theta_\mathrm{min}}{\pi - \theta_\mathrm{max}} \frac{\theta_n + \theta_\mathrm{i} - (\pi - \theta_\mathrm{max})}{\theta_n + \theta_\mathrm{i} - (\pi - \theta_\mathrm{min})}\right| \mathrm{d}\theta_\mathrm{i}. \tag{27}$$

However, Eq. 27 is a non-elementary integral as it can be expressed in terms of dilogarithm functions [7]. Taking also the complicated integration domain I into account, a closed-form solution appears to be inaccessible. Nevertheless, with the assumptions used for the irregularity bounds in Eq. 26, it is easy to recognize that the same asymptotic slope a as for the regular case is recovered, since Eq. 27 converges to Eq. 13 as $\theta_\mathrm{i}^-, \theta_\mathrm{i}^+ \to 0$, which is the case for $n \to \infty$. The asymptotic intercept b, on the other hand, depends on the granted range of irregularity.

In order to calculate m_n for given n, we evaluate the double integral numerically using the acceptance-rejection method with uniform sampling in the domain $[\theta_\mathrm{i}^-, \theta_\mathrm{i}^+] \times [\underline{\theta}, \overline{\theta}]$ in MATLAB 2018a. The integral offers sufficient parametric freedom to get very close to the linear Aboav–Weaire relationship over the entire range of polygon types (Fig. S6), and it still does if $\underline{\theta} = 0$ is fixed, such that the lower integration bound θ_min is essentially governed by the symmetry requirement of θ_1 and θ_2. Furthermore, restricting the irregularity angles to symmetric domains by setting $\alpha = \beta$ leaves us with two free parameters, $\overline{\theta}$ and β. A curve fit of our model to the empirical line $mn = an + b$ with $a = 5$ and $b = 8$ yields least squared errors for $\overline{\theta} = 151.3 \pm 0.7°$ and $\beta = 0.59 \pm 0.04$ with an adjusted coefficient of determination of $\overline{R}^2 = 0.997$ (Fig. S6). Taking the mean epithelial coefficients $a = 4.8$, $b = 8$ (see Fig. 2c in the main article) as a reference, we find $\overline{\theta} = 146.3 \pm 0.5°$ and $\beta = 0.52 \pm 0.03$ ($\overline{R}^2 = 0.998$), both of which are physiologically plausible values for epithelial tissue.

In summary, the linear Aboav–Weaire law emerges naturally for geometric reasons in contiguous, two-dimensional cellular lattices when a limitation in locally available cell areas and matching side lengths enforce polygonal irregularity, i.e., interior angles deviating from those of regular polygons. For high-n polygons ($n > 6$), it can even be explained by the cells' tendency toward regular polygonal shapes alone. We expect this explanation of Aboav–Weaire's law to be applicable also to other systems partially driven by surface minimisation and area variability, such as soap bubble froths or polycrystals. Our theoretical results might also be appreciable in terms of contact graph theory, of which the present polygonal space-filling packing represents a special case.

2 `LBIBCell` Simulations

Simulation framework We used the software `LBIBCell` [15] to simulate the detailed epithelial tissue dynamics. `LBIBCell` simulates a 2D plane of the epithelial tissue, and thus allows us to simulate the apical cell dynamics, or more precisely a plane where cells adhere laterally (Fig. 2a, main manuscript). `LBIBCell` represents the extracellular and cytoplasmic spaces of the tissue as Newtonian fluids and incorporates the fluid-structure interaction with the elastic cell boundaries via an immersed boundary method [10]. The Navier-Stokes equation for the fluid dynamics is solved using the Lattice Boltzmann method, i.e., the fluid and its motion are realised by particle ensembles which stream and collide on a 2D regular lattice [2]. Cell boundaries are geometrically highly resolved and cell boundaries and cell-cell junctions are modelled with elastic springs.

`LBIBCell` **Simulations for Figure 2** The proliferating *Drosophila* larval wing disc tissue was simulated as described in (Kokic et al, submitted); the parameter values are summarised in Table S1. Simulations with two different cell division rules were carried out 10 times each. According to the first cell division rule, Hertwig's rule [5,3,8], cells divide perpendicular to their longest axis. In the second set of simulations, the orientation of the cell division axis was randomised. Details on the implementation of the cell division rules can be found in [15].

`LBIBCell` **Simulations for Figure 3** To generate polygonal lattices of regular polygons, centres of circular cells were placed at sites corresponding to the centres of regular polygons in different Euclidean tilings by convex regular polygons (i.e., $\{6,6,6\}$, $\{4,8,8\}$, $\{4,6,12\}$, $\{3,12,12\}$). The relative sizes of the cells followed the quadratic law (Eq. 3 in the main manuscript). In a second step, the circular cells were enlarged uniformly until they collided at single points with their neighbours. These start structures (`LBIBCell` input) were created using Inkscape [6], Fiji [13,14] and R [16]. A detailed description of the pipeline and scripts are available on `https://git.bsse.ethz.ch/iber/Publications/2019_vetter_kokic_aboav-weaire-law`. In a last step, cells were grown uniformly until the entire lattice was filled with cells and cells thus formed a contiguous lattice. In order to prevent gaps, the cell junction search radius was increased to its maximum value (cf. Figure S3 in Kokic et al., submitted; Table 1), and the amount of mass that was added intracellularly was subtracted from the extracellular fluid (cf. `Cell Junction` and `Membrane Channels` in Table S1). All other `LBIBCell` parameter values were set to the same values as for the *Drosophila* larval wing disc (Table S1), and all subsequent quantifications were carried out as described in (Kokic et al., submitted).

3 Supplementary Tables

Table S1: **Parameter values for the simulation of *Drosophila* larval wing disc epithelia.** Parameters in grey-highlighted rows only affect the numerical accuracy of the simulations. The other parameter values are specific to the biological problem of interest, and were determined based on published quantitative data for the *Drosophila* larval wing disc pouch (Kokic et al, submitted). This table is reproduced with modifications from (Kokic et al, submitted).

`LBSolver`	Parameter Description	Value [LB units]	Value [SI units]	Determination / Literature
	τ_{fluid} - relaxation time	2	N/A	[11]
`BioSolver`	Parameter Description	Value [LB units]	Value [SI units]	Determination / Literature
`Cell Growth`	frequency of applying `BioSolver`	1:1	N/A	(Kokic et al, submitted)
	I - total number of iterations	64300 / 150000	24-96h AEL / 0-168h AEL	(Kokic et al, submitted)
	b - Gompertz constant	11.331	11.331	[9]
	τ - Gompertz constant	0.8555	143.7773h/168h	[9]
`Membrane Tension`	frequency of applying `BioSolver`	1:10	N/A	(Kokic et al, submitted)
	Hookean spring constant	0.01	N/A	[4]
`Cell Junction`	frequency of applying `BioSolver`	1:10	N/A	(Kokic et al, submitted)
	search radius for junction building	1.0	N/A	
	length of intercellular cell junction	0.3	27nm	16-39nm [12]
	Hookean spring constant	0.1	N/A	[4]
`Cell Division`	frequency of applying `BioSolver`	1:1000	N/A	(Kokic et al, submitted)
	maximal cell area	1771	$14.1\mu\text{m}^2$	[4]
	mean cell division threshold	837	$7\mu\text{m}^2$	[4]
	std cell division threshold	256	$2\mu\text{m}^2$	[4]
`Cell Extrusion`	frequency of applying `BioSolver`	1:100	N/A	(Kokic et al, submitted)
	minimal cell area	100	$0.8\mu\text{m}^2$	[15, 4]
`Membrane Channels`	frequency of applying `BioSolver`	1:1	N/A	[15]
	growth source	0.01	N/A	[15]

References

[1] David A. Aboav. The arrangement of grains in a polycrystal. *Metallography*, 3(4):383–390, 1970.

[2] Shiyi Chen and Gary D. Doolen. Lattice Boltzmann Method for Fluid Flows. *Annual Review of Fluid Mechanics*, 30(1):329–364, 1998.

[3] William T. Gibson, James H. Veldhuis, Boris Rubinstein, Heather N. Cartwright, Norbert Perrimon, G. Wayne Brodland, Radhika Nagpal, and Matthew C. Gibson. Control of the mitotic cleavage plane by local epithelial topology. *Cell*, 144(3):427–438, 2011.

[4] Davide Heller, Andreas Hoppe, Simon Restrepo, Lorenzo Gatti, Alexander L. Tournier, Nicolas Tapon, Konrad Basler, and Yanlan Mao. EpiTools: An Open-Source Image Analysis Toolkit for Quantifying Epithelial Growth Dynamics. *Developmental Cell*, 36(1):103–116, 2016.

[5] Oskar Hertwig. *Das Problem der Befruchtung und der Isotropie des Eies, eine Theorie der Vererbung*. Jenaische Zeitschrift für Naturwissenschaften. Fischer, 1884.

[6] Inkscape Project. https://inkscape.org.

[7] Leonard Lewin. *Polylogarithms and associated functions*. Elsevier North Holland, New York, 1981.

[8] Nicolas Minc, David Burgess, and Fred Chang. Influence of cell geometry on division-plane positioning. *Cell*, 144(3):414–26, 2011.

[9] Ulrike Nienhaus, Tinri Aegerter-Wilmsen, and Christof M. Aegerter. *In Vivo* imaging of the Drosophila wing imaginal disc over time: Novel insights on growth and boundary formation. *PLoS ONE*, 7(10):e47594, 2012.

[10] Charles S. Peskin. The immersed boundary method. *Acta Numerica*, 11:479–517, 2002.

[11] Yue-Hong Qian, Dominique d'Humières, and Pierre Lallemand. Lattice BGK models for Navier-Stokes equation. *EPL (Europhysics Letters)*, 17(6):479, 1992.

[12] Christoph A. Reinhardt and Peter J. Bryant. Wound healing in the imaginal discs of Drosophila II. Transmission electron microscopy of normal and healing wing discs. *Journal of Experimental Zoology*, 216(1):45–61, 1981.

[13] Johannes Schindelin, Ignacio Arganda-Carreras, Erwin Frise, Verena Kaynig, Mark Longair, Tobias Pietzsch, Stephan Preibisch, Curtis Rueden, Stephan Saalfeld, Benjamin Schmid, et al. Fiji: an open-source platform for biological-image analysis. *Nature Methods*, 9(7):676, 2012.

[14] Caroline A Schneider, Wayne S Rasband, and Kevin W Eliceiri. Nih image to imagej: 25 years of image analysis. *Nature Methods*, 9(7):671, 2012.

[15] Simon Tanaka, David Sichau, and Dagmar Iber. LBIBCell: a cell-based simulation environment for morphogenetic problems. *Bioinformatics*, 31(14):2340–2347, 2015.

[16] R Core Team et al. R: A language and environment for statistical computing. 2013.

[17] Denis Weaire. Some remarks on the arrangement of grains in a polycrystal. *Metallography*, 7(2):157–160, 1974.